JOURNAL OF AIRCRAFT
Vol. 33, No. 4, July–August 1996

Flat Spin of a Circular Cylinder

L. E. Ericsson*
Mountain View, California 94040
and
M. E. Beyers†
Institute for Aerospace Research, Ottawa, Ontario K1A 0R6, Canada

Experimental results are analyzed to develop an understanding of the flow physics causing flat spin of circular cylinders in the critical Reynolds number region. The analysis shows that the flow phenomenon playing the key role in producing flat spin is a three-dimensional moving wall effect, which becomes especially powerful in the critical flow region by controlling flow separation through its effect on boundary-layer transition. Three-dimensional flow phenomena appear to establish the spanwise venting needed to sustain the asymmetric flow separation. It is also found that three-dimensional nonuniform roughness as well as body microasymmetry play important roles in initiating the flat-spin motion.

Nomenclature

D' = crossflow drag, coefficient $c_D = D'/(\rho_\infty U_\infty^2/2)dl$
d = cylinder diameter
h = height of protuberance
L = cylinder lift, coefficient $C_L = L/(\rho_\infty U_\infty^2/2)dl$
l = cylinder length
N = flat spin rate
n = yawing moment, coefficient $C_n = n/(\rho_\infty U_\infty^2/2)Sl$
P = static pressure, coefficient $C_p = (P - P_\infty)/(\rho_\infty U_\infty^2/2)$
p = spin rate
Re = Reynolds number, $U_\infty d/\nu_\infty$
S = reference area, $\pi d^2/4$
t = time
U = velocity
Y' = sectional side force, coefficient $c_y = Y'/(\rho_\infty U_\infty^2/2)d$
y = spanwise coordinate
α = angle of attack
Δ = increment
δ = roughness height
η = dimensionless y coordinate, $2y/l$
ν = kinematic viscosity
ρ = fluid density
ϕ = azimuthal angle
ϕ_0 = azimuth of flow stagnation point
Ω = dimensionless flat spin rate, $\pi Nl/U_\infty$

Subscripts
b = base
cr = critical
FS = flat spin
r = resultant
w = wall
∞ = freestream conditions

Introduction

THE flat spin of a circular cylinder presents a problem for circular canisters dropped from sounding rockets as the g-loads are potentially destructive for the instrumentation payload. The circular cylinder in flat-spin motion exhibits fluid phenomena that are fundamental to bodies of revolution in general[1] and, therefore, have relevance to forebodies of aircraft in flat spin. It has been shown that at high angles of attack (AOA) the so-called moving wall effect[2] on flow separation can drive a body in a coning motion. This has been observed experimentally,[3] demonstrating that the moving wall effects will dominate over the effects of geometric microasymmetries.[4] The effects of flow separation are especially powerful in the critical flow region, when they act on boundary-layer transition.[2] This is of particular interest as, during the descent through the atmosphere, the Reynolds number of the full-scale canister passes through the critical range. The aim of this article is to identify the three-dimensional flow mechanism in flat spin, in particular to define how it changes the role of the moving wall effect from what it is in the case of self-excited coning[5] at $\alpha << 90$ deg.

Preliminary Considerations

For a perfectly smooth axisymmetric body, free to spin around the wind axis, the coning direction would be determined by external perturbations of some sort, such as flow nonuniformity or unsteadiness.[3-5] The same is true for the flat-spin direction of a circular cylinder with the rotation axis located at midbody. Static tests of an $l/d = 3.82$ circular cylinder[6] showed a side force developing in the critical Reynolds number region (Fig. 1a), where the asymmetric, one-bubble flow separation geometry has been observed in two-dimensional tests[7] (Fig. 1b). If the asymmetry were the same across the span for the finite l/d cylinder[6] as in the two-dimensional test,[7] no yawing moment and, consequently, no flat spin would develop around a midbody rotation axis.

The fact that flat spin does develop[6,8] indicates that the static side force (Fig. 1a) is not symmetrically distributed along the span at or near the critical Re region. There are several possible causes, including nonuniform roughness distribution, body microasymmetry, and support-induced flow asymmetry. Once the flat-spin motion is initiated, moving wall effects apparently play the dominant role[9] as in the case of the coning motion,[3,4] judging by the pressure measurements on a circular cylinder driven at 500 rpm around the midbody axis at $Re = 0.318 \times 10^6$ (Ref. 6 and Fig. 2). The local rotation-induced moving wall effects produced the critical–supercritical flow asymmetry in opposite directions on the two sides of the rotation axis[6] (Fig. 3). In Fig. 2 the stagnation point for section $Q - Q$ is at $\phi \approx 30$ deg, corresponding to $\phi = 0$ in the flow sketch in Fig. 3.

Presented as Paper 94-0158 at the AIAA 32nd Aerospace Sciences Meeting and Exhibit, Reno, NV, Jan. 10–13, 1994; received Dec. 10, 1994; revision received March 26, 1996; accepted for publication April 3, 1996.

*Engineering Consultant. Fellow AIAA.
†Head Aerodynamics Group, Aerodynamics Laboratory. Senior Member AIAA.

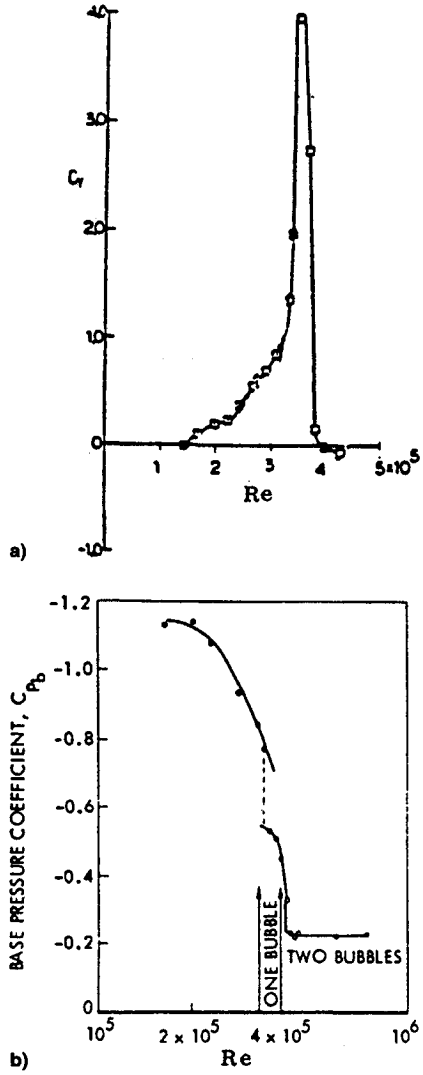

Fig. 1 Aerodynamic characteristics of a circular cylinder in the critical Reynolds number region: a) measured side force on *l/d* = 3.82 circular cylinder[6] and b) pressure distribution on a two-dimensional cylinder.[7]

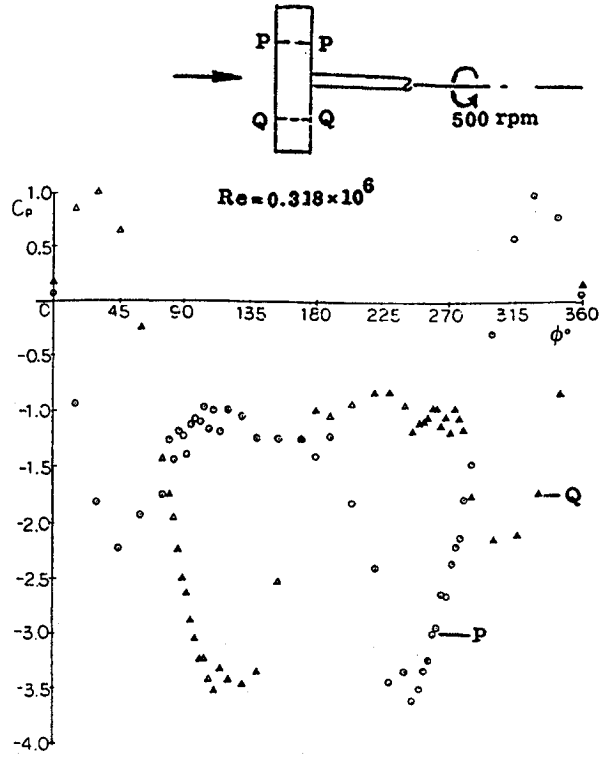

Fig. 2 Pressure distribution on a circular cylinder in flat-spin motion at $Re = 0.318 \times 10^6$ and $N = 500$ rpm.[6]

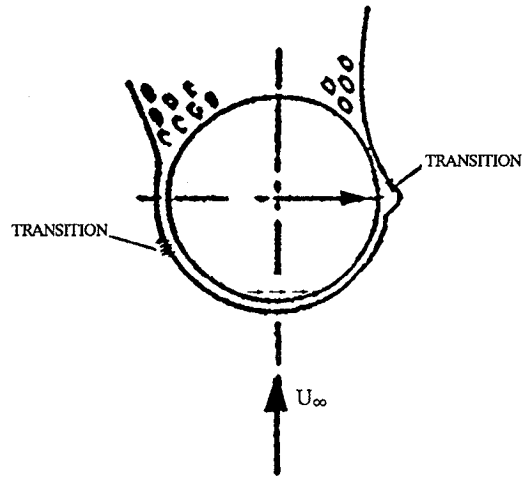

Fig. 3 Supercritical–critical crossflow separation on a translating cylindrical cross section.

The downstream moving wall effect delays transition enough to keep the critical flow separation with its laminar separation bubble. The reattaching turbulent boundary layer separates at roughly 140-deg azimuth,[9,10] i.e., at $\phi \approx 140 - 30 = 110$ deg in Fig. 2 for section $Q - Q$. In Fig. 3 the upstream moving wall effect has moved the transition forward of the laminar separation bubble, wiping it out on that side. The resulting supercritical separation occurs at roughly 110-deg azimuth.[9,10] This corresponds to $\phi \approx 360 + 30 - 110 = 280$ deg for section $Q - Q$ in Fig. 2. Considering the data accuracy, the experimental results in Fig. 2 are in good agreement with the postulated supercritical–critical crossflow separation geometry shown in Fig. 3, which generates a prospin yawing moment. The steady-state flat-spin results when this prospin moment is balanced by the antispin moment generated by the crossflow drag.[9]

Moving Wall Effect

The moving wall effect becomes extremely large when it affects flow separation via boundary-layer transition. This is demonstrated by the experimental Magnus lift characteristics[11] shown in Fig. 4. At $Re = 0.128 \times 10^6$, increasing the rotation rate past the critical value to $U_W/U_\infty \geq 0.3$ (curve f in Fig. 4) results in Magnus lift reversal, producing an almost instantaneous loss of lift, $\Delta C_L \approx -0.3$. When the Reynolds number is increased to the critical value, $Re \approx 0.3 \times 10^6$ (curve k in Fig. 4), the moving wall effect acts on the shear-layer transition in the laminar separation bubble, greatly increasing the magnitude of the Magnus lift reversal; $\Delta C_L \approx -0.6$ compared to $\Delta C_L \approx -0.3$. That the lift loss does not reach the magnitude, $0.8 \leq |\Delta C_L| \leq 1.2$, indicated by static measurements[12] (Fig. 5), is probably attributable to the increased suction lift generated on the top side through the delay of the laminar flow separation caused by the downstream moving wall effect.[3]

Three-Dimensional Flow Effects

One big difference between three- and two-dimensional results is found in the measured side force and lift, respectively, below the critical flow conditions. This is the likely result of nonuniform roughness distribution and turbulence. The systematic two-dimensional tests performed by Schewe[13] (Fig. 6) show that the flow separation is laminar, subcritical, at $Re = 2 \times 10^5$, critical at $Re = 3 \times 10^5$, where a symmetric as well as

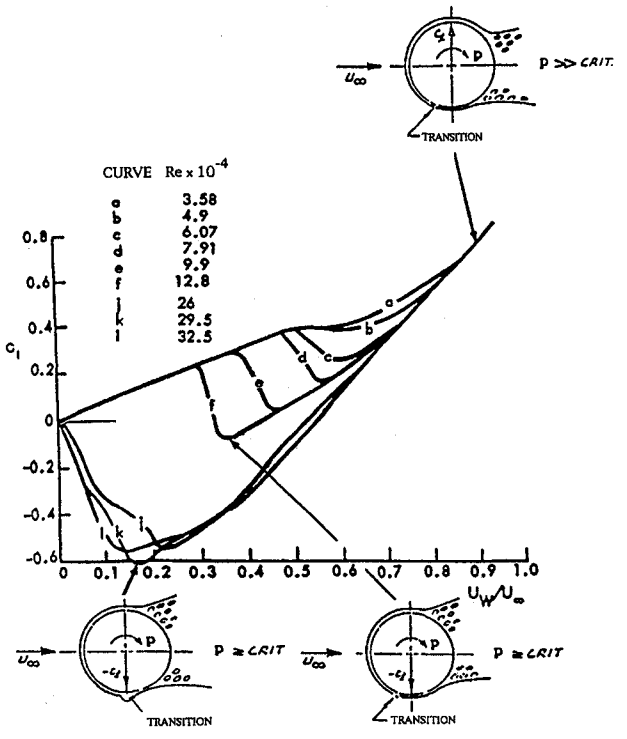

Fig. 4 Magnus lift of a rotating circular cylinder at critical and initially subcritical flow conditions.[11]

two alternative asymmetric critical-flow separation geometries were observed, and, finally, supercritical at $Re = 4 \times 10^5$. The oil flow visualization results shown in Fig. 6 confirm the results obtained by Kamiya[12] (Fig. 5). In Schewe's test[13] the Reynolds number was adjusted so that natural boundary-layer transition could be expected to occur. The top graph in Fig. 7 shows a transition from symmetric, supercritical to asymmetric, critical flow separation, and the bottom one shows a transition from symmetric, subcritical to asymmetric, critical flow separation. That is, the Reynolds number was, respectively, decreased and increased to the critical value. The direction of the separation asymmetry was investigated 28 times, showing that there was no preference. Both directions were equally probable, regardless of whether the Reynolds number was increasing or decreasing. The resulting separation asymmetry was very stable in both cases. The time Δt required to establish the separation asymmetry was an order of magnitude larger than the period of the von Kármán vortex shedding.

Roughness Effects

The characteristics in Fig. 7 could also be produced by using a triggering device[13] (Fig. 8). The pin had a diameter of 0.8 mm, compared to the cylinder diameter of 60 mm. The height was $h \leq 1$ mm. To trip the transition, the pin had to be located between 45 and 60 deg azimuth from the stagnation point. The transition from symmetric, subcritical to asymmetric, critical flow separation did not always cover the whole span, resulting in $|\Delta C_L| < 1$. However, once complete flow separation asymmetry was established, retracting the pin had no effect. The sign of the separation asymmetry was determined by the pin

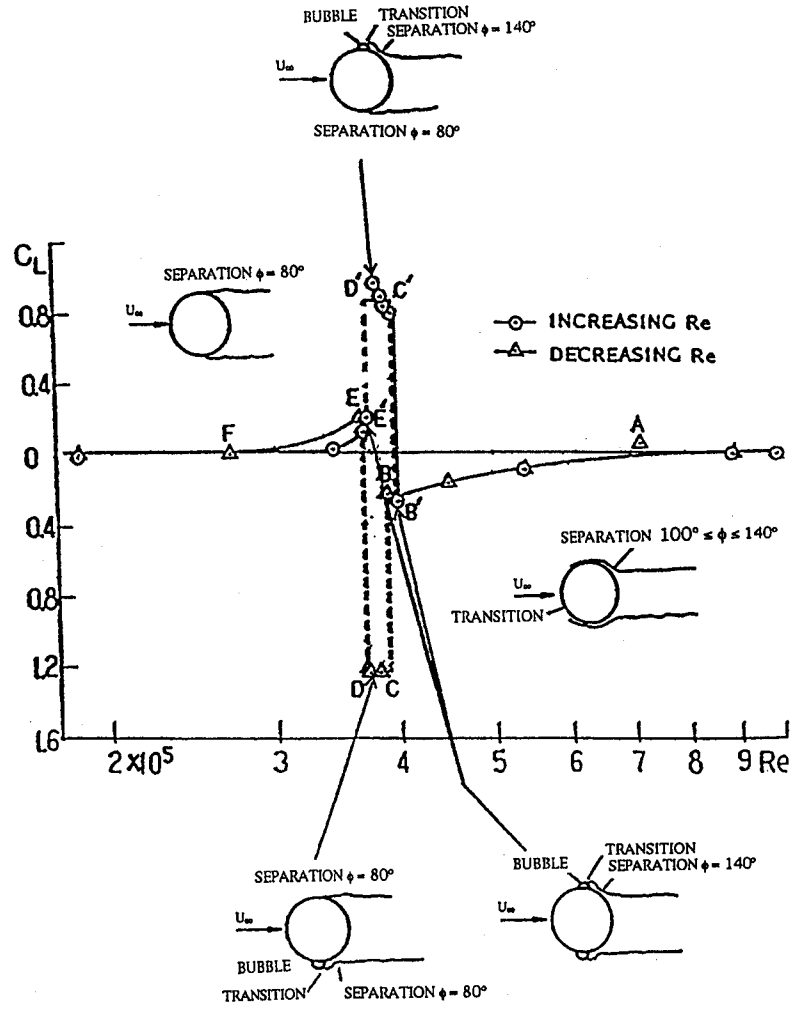

Fig. 5 Static lift of a circular cylinder in the critical Reynolds number region.[12]

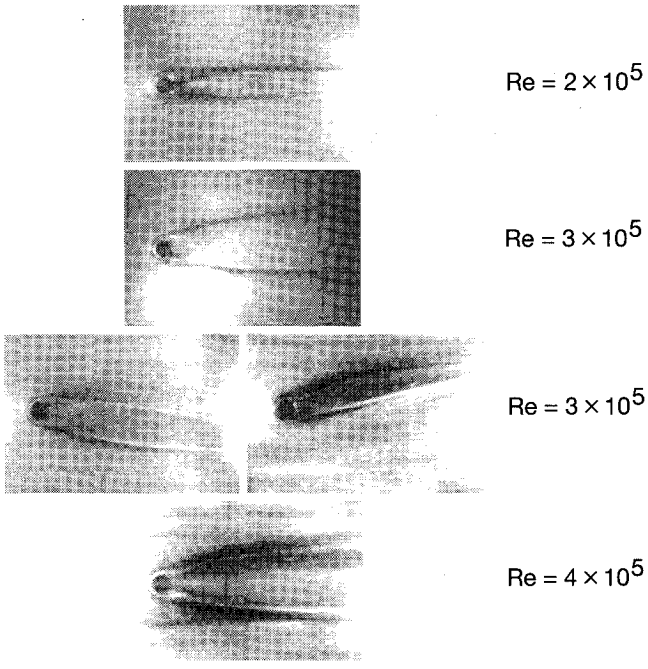

Fig. 6 Flow visualization of the crossflow over a circular cylinder at subcritical, critical, and supercritical flow conditions.[13]

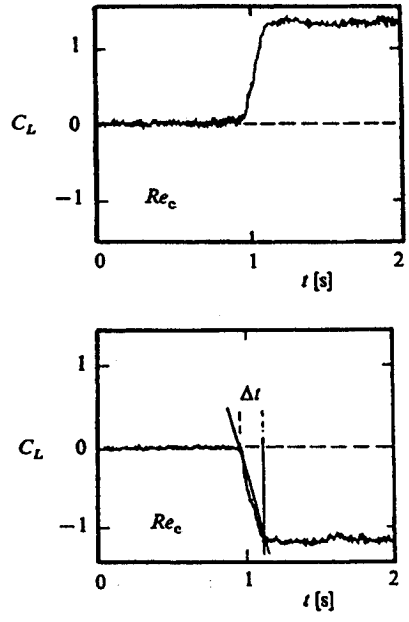

Fig. 7 Lift of a circular cylinder at critical flow conditions for increasing and decreasing Reynolds number.[13]

location. Perturbing the upper side gave positive lift for increasing Re and negative lift for decreasing Re. Thus, for the same pin location, the separation asymmetry depends upon whether the Reynolds number is increasing or decreasing, i.e., whether the symmetric flow separation is subcritical or supercritical, respectively. In the former case the protuberance promoted transition, establishing the critical type of flow separation on the top side, producing a strong turbulent boundary layer with associated greatly delayed flow separation, resulting in positive lift generation. In the supercritical case, the protuberance simply promoted the supercritical nature of the flow separation on the top side, moving it back toward $\phi = 100$ deg.[9,10] This allows the critical flow separation to be established on the opposite, bottom side, resulting in negative lift generation through the crossflow separation geometry sketched in Fig. 3. In flat spin, the upstream moving wall effect produces very similar results, promoting transition, either through the subcritical/critical crossflow separation, shown in Fig. 4 for $U_W/U_\infty < 0.1$, or the supercritical/critical flow separation, shown in Fig. 3.

On the actual free-falling canister, the roughness might take the form of a distribution of surface depressions and protuberances. The presence of dimples is equally effective in lowering the critical Reynolds number.[14] Little, if any, data are available to compare the effects of a single roughness element (such as that in Fig. 8) with those of distributed roughness. However, since the key factor is the location of a roughness element in a certain azimuthal region, the presence of local distributed roughness in that region should result in continuous triggering of the separation asymmetry on the cylinder in flat-spin motion.

Combining these results with the experimentally observed[13] arbitrary direction of the separation asymmetry on a smooth circular cylinder, one concludes that it must be a combination of local roughness, local Reynolds number, and local turbulence that determines the initial direction of the flow separation asymmetry. How extremely sensitive the Reynolds number

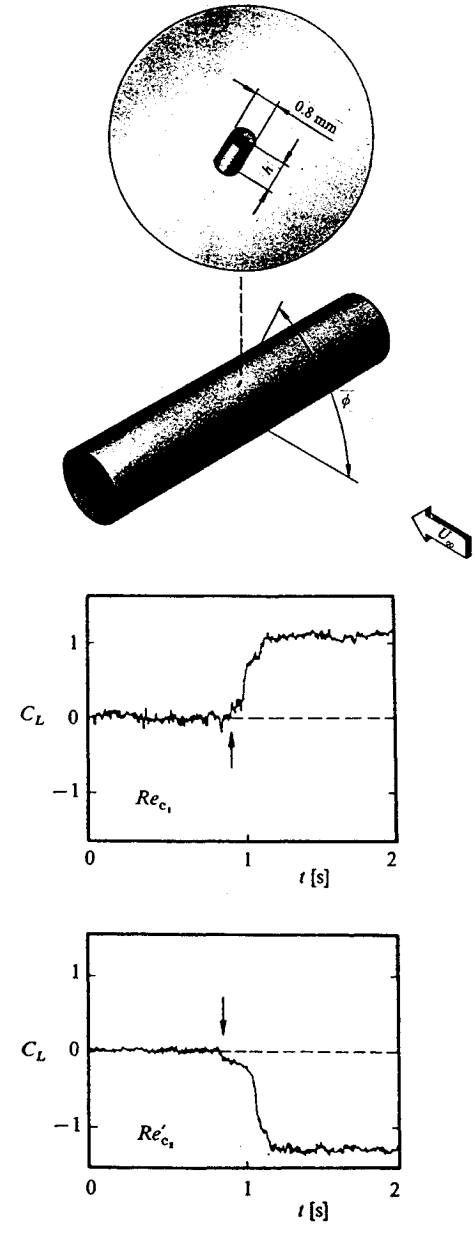

Fig. 8 Lift of a circular cylinder controlled by a cylindrical protuberance.[13]

boundaries of the critical flow regime are to roughness effects is demonstrated by the experimental results[15] in Fig. 9. Even with the definition of smooth used by Schechenyi,[16] i.e., $(\delta/d)_{\text{smooth}} \leq 3.3 \times 10^{-4}$, Fig. 9 indicates that the critical regime extends from $Re = 1.8 \times 10^5$ to $Re = 5.7 \times 10^5$.

In Schewe's cylinder experiment[13] the separation asymmetry for initially symmetric, subcritical flow separation was in some cases established only over part of the span. In the three-dimensional flow case of flat spin, spanwise venting exists in the separated flow region, starting somewhere near midbody in the static case, definitely at the midbody in the flat-spin case. Thus, it is no surprise that a side force was measured[9] by Kubota et al.[6] before the critical Reynolds number was reached (Fig. 1a). Based upon these results the flat-spin data[6] in Fig. 10 show that the critical flow condition was established early on one-half (spanwise) of the cylinder at $Re < 3 \times 10^5$. That would explain the lower spin rate plateau compared to $Re > 3 \times 10^5$, when the critical flow condition supposedly is established on both (spanwise) halves. The Re hysteresis is a result of the same type of flow–inertia effect that kept the separation asymmetry in Fig. 8 when the pin was retracted. As expected,

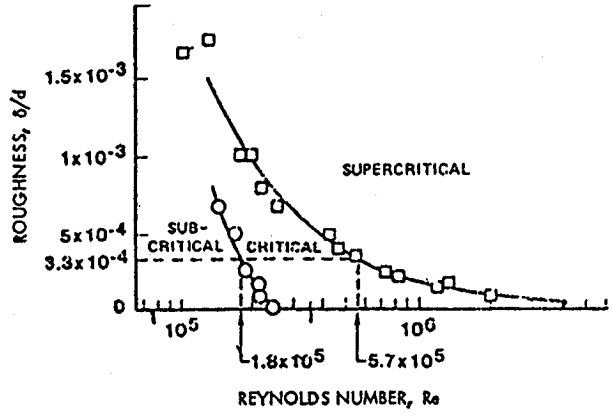

Fig. 9 Effect of roughness on the extent of the critical Reynolds number region.[15]

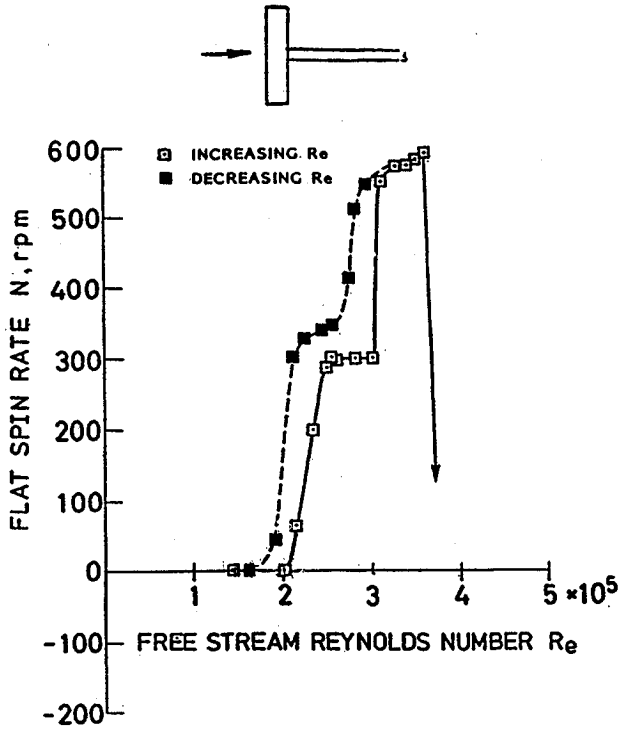

Fig. 10 Flat spin of a circular cylinder for increasing and decreasing Reynolds number.[6]

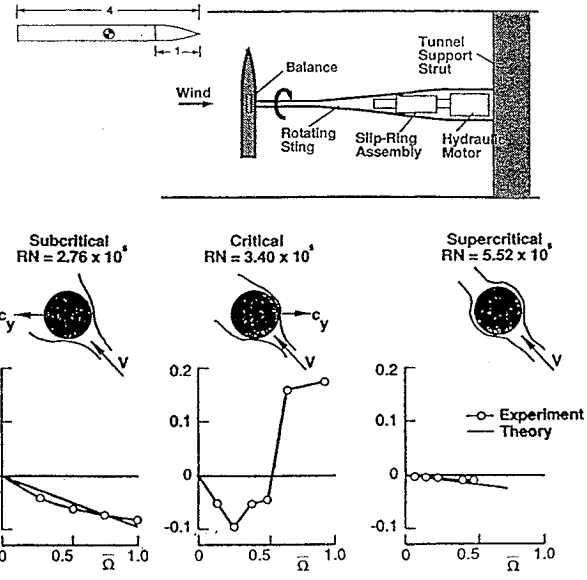

Fig. 11 Yawing moment for forced flat spin at subcritical, critical, and supercritical flow conditions.[17]

the Re hysteresis occurs in both cases, $Re < 3 \times 10^5$ as well as $Re > 3 \times 10^5$.

Prediction of Flat Spin Using Static Data

In an exploratory project to develop methods for prediction of flat spin, NASA Langley Research Center generated the results[17] presented in Fig. 11. Using the two-dimensional drag, where $c_D \approx 1.2$ in the subcritical region, $Re < 0.3 \times 10^6$, and $0.3 < c_D < 0.4$ in the supercritical region, $Re > 0.4 \times 10^6$ (Ref. 17). It can be seen that using these values in a strip analysis gave a rather good prediction of the flat-spin (yawing) moment C_n as a function of the reduced spin rate $\Omega = \pi Nl/U_\infty$. (For the midbody rotation axis $\Omega = U_{W\max}/U_\infty$.) However, the static data cannot predict the measured C_n in the critical flow region, where the moving wall effects dominate.[2] Actually, all three sets of test results in Fig. 11 require further explanation.

As the contribution to the yawing moment from a local segment is proportional to the square of the spanwise distance from the rotation center,[9] it is the circular–cylinder portion of the ogive–cylinder in Fig. 11 that generates the important aerodynamics. Consequently, the results in Fig. 11 are of direct interest for the present case of flat spin of a circular cylinder. Based on the results for a body in steady coning motion at subcritical flow conditions,[3,4] one would expect the measured C_n to be positive at low Ω, and to become zero at a certain Ω. Why are the undamping moving wall effects causing the steady-state coning absent in the flat-spin results[17] in Fig. 11?

Three-Dimensional Flow Mechanisms in Flat Spin

Spanwise Flow Venting

On the coning body at $\alpha < 60$ deg the static axial flow component provides the venting of the separated flow region that is needed to establish steady asymmetric flow separation.[4] No corresponding flow component exists in the flat spin. The flow mechanism providing a spanwise flow component on the cylinder in flat spin is governed by the three dimensionality of the rotational flowfield. A nonplanar velocity distribution exists as a result of the helical stagnation line, which can be understood from kinematic considerations (Fig. 12). At the spanwise station η the angle ϕ_0 is

$$\phi_0 = \tan^{-1}(\eta\Omega) \tag{1}$$

At flat spin, $\Omega = \Omega_{FS} \approx \pm 1$, and Eq. (1) gives

$$\phi_0 = \pm\tan^{-1}(\eta\Omega_{FS}) \approx \pm\tan^{-1}\eta \qquad (2)$$

Stations $P - P$ and $Q - Q$ in Fig. 2 are at $\eta = \pm 0.5$, which in Eq. (2) gives $\phi_0 = \pm 26.5$ deg. This agrees reasonably well with the experimental results in Fig. 2, $\phi_0 \approx \pm 30$ deg. At the cylinder tips, $\eta = \pm 1$ and Eq. (2) yields $\phi_0 = \pm 45$ deg. The separation asymmetry is skewed by the helix angle ϕ_0 (see inset sketch in Fig. 12). Thus, the local side force, as determined by two-dimensional strip analysis, is not in the plane of the flat spin. The experimental results in Fig. 2 show supercritical separation to occur at $60 < \phi < 80$ deg, i.e., 90–110 deg from the flow stagnation point. The critical separation occurs at $160 < \phi < 180$ deg, i.e., 130–150 deg from the flow stagnation point. In two-dimensional flow over a stationary circular cylinder the supercritical and critical flow separations occur at approximately 110 and 140 deg azimuth, respectively.[9,10] That is, the experimental results in Fig. 2 suggest that the upstream moving wall effect promoted the supercritical separation to occur earlier than on the stationary cylinder, and the downstream moving wall effect delayed the critical separation, all in agreement with expectations.[2] Thus, the moving wall effects produce an additional twist of the crossflow separation in addition to the spin-induced skewing of the flow stagnation line, an effect neglected in Ref. 9. The analysis in Ref. 9 accounts only for the helical skewing of the flow stagnation line when using two-dimensional experimental Magnus lift results[11] to account for the moving wall effects. On the outboard sections near the cylinder tips, the contributions to the autorotative moment are reduced greatly through three-dimensional end effects, including the effect of tip vortices, generating an influence of the finite span somewhat similar to that for a wing.[9]

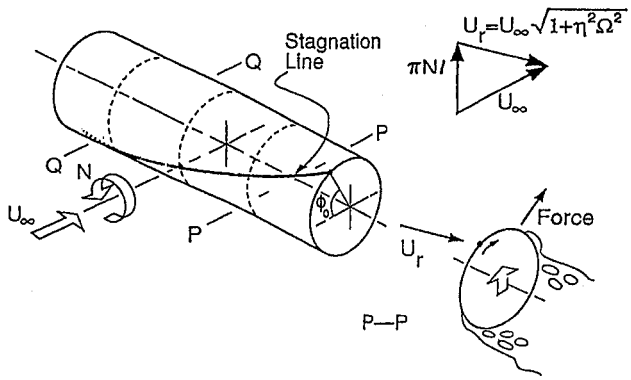

Fig. 12 Helical flow stagnation line on a circular cylinder in flat spin.

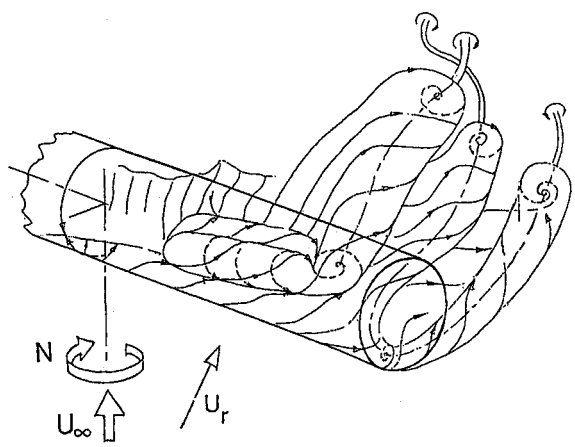

Fig. 13 Conceptual flowfield on a circular cylinder in flat spin at critical Reynolds numbers.

The location and size of a laminar separation bubble is governed by three-dimensional flow effects. As a result of the spanwise pressure gradient caused by the rotation-induced flow separation asymmetry, sketched in Fig. 12, vortex splitting is likely to occur, similar to that observed on a stationary cylinder at transitional Reynolds numbers.[18] To quote the authors: "Two-dimensional laminar separation with twin-separation lines is observed at a subcritical Reynolds number at $Re = 1.85 \times 10^5$. Three-dimensional, cell-like separation is found beyond the critical Reynolds number at $Re = 4.1 \times 10^5$." This cell-like structure will also exist for the flat-spin case, but deformed through the helical skewing. That is, streamwise vortices are venting the separation bubbles, with a single cell appearing on each half-span of the cylinder, locked into position by the spanwise local Reynolds number variation and pressure gradients (Fig. 13). The streamwise vortices on the outboard end of the separation bubble will interact, and possibly combine with the tip vortices. This could provide the spanwise venting needed to maintain the asymmetric crossflow separation geometry.

Von Kármán Vortex Shedding

Another important difference between the coning and flat-spin motions is that unsteady von Kármán vortex shedding is only present for the flat-spin case. For subcritical flow conditions ($Re \leq 0.128 \times 10^6$ in Fig. 4) the oscillatory forces caused by von Kármán vortex shedding are of the same magnitude as the measured Magnus lift on a rotating circular cylinder.[12,19] For the rotating circular cylinder in Fig. 4, the steady moving wall effects are apparently strong enough to rotate the flow separation to produce a nonzero time average in presence of the von Kármán vortex shedding. This occurs because the moving wall effects interact with the boundary layer up to the flow separation point. In contrast, on the cylinder in flat spin the moving wall effects are concentrated in the boundary-layer build-up region near the flow stagnation point and cannot compete with the forced oscillation of the separation point through the von Kármán vortex shedding, resulting in zero time-averaged side force. A similar condition exists at supercritical flow conditions. However, von Kármán vortex shedding with a unique Struhal number such as in the case of subcritical or supercritical flow conditions, does not exist at critical flow conditions.[20] Consequently, the steady-state moving wall effects could be overmatched by the forced oscillation of the separation point through the von Kármán vortex shedding, resulting in zero time-averaged side force through asymmetric crossflow separation; this leaves the damping crossflow drag in full control, as indicated by the experimental results for $Re = 2.76 \times 10^5$ and $Re = 5.52 \times 10^5$ in Fig. 11.

The deviation from prediction of the experimental results in Fig. 11 could be caused by the variation of the local Reynolds number along the span, in addition to any three-dimensional flow effects. As the local Reynolds number is $Re = Re(1 + \eta^2\Omega^2)^{1/2}$, one can see that the maximum local Reynolds number for $\Omega = 1$ is $Re_{max} = Re(1 + \eta^2)^{1/2}$. Thus, for $Re = 2.76 \times 10^5$ one obtains $Re_{max} = 3.8 \times 10^5$ at the cylinder tip ($\eta = 1$), i.e., well into the critical flow region. Thus, the variation of cylinder drag with Reynolds number[21] could produce the subcritical experimental data trend in Fig. 11. For the supercritical case, $Re > 4.3 \times 10^5$, the drag is only $c_D \approx 0.3$, resulting in the diminutive $C_n(\Omega)$ shown in Fig. 11 for $Re = 5.52 \times 10^5$.

Forced Flat Spin

The most intriguing results from the flat-spin test[17] (Fig. 11) are those shown in Fig. 14 for the critical flow conditions. To understand them it is again helpful to revisit the Magnus lift results[11] in Fig. 4. At $U_W/U_\infty < 0.1$, the moving wall effect delays shear-layer transition in the laminar separation bubble on the top side and promotes transition in the bubble on the bottom side (see bottom inset in Fig. 14). As a consequence, the final, turbulent flow separation is delayed more on the bot-

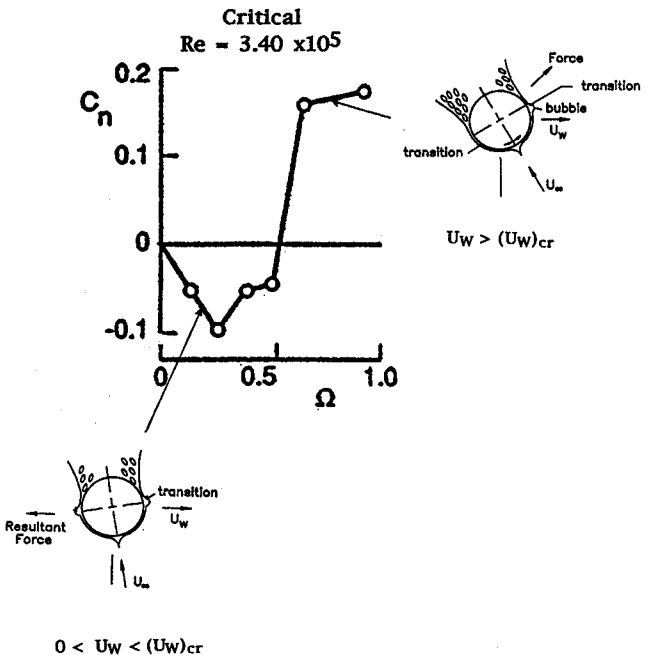

Fig. 14 Yawing moment measured at critical flow conditions.[17]

tom side than on the top side,[2] resulting in the measured[11] negative Magnus lift. In the flat-spin case under critical flow conditions (Fig. 14), the moving wall effect on the two-bubble separation geometry will also generate a negative force, resulting in a negative yawing moment, as illustrated in Fig. 14 for $\Omega <$ 0.25. Note that the drag-generated contribution to C_n is of much smaller magnitude than at subcritical flow conditions, $c_D < 0.3$ compared to $c_D \approx 1.2$. Consequently, the antispin moment C_n in Fig. 14 for $\Omega < 0.25$ is largely generated by the critical/critical crossflow separation. Comparing Fig. 14 with Fig. 4, one can see that in the three-dimensional case there is a complicated transition to the final one-bubble geometry (Fig. 3) that is not present in the two-dimensional case. Clearly, this difference is caused by the three-dimensional flow effects discussed earlier, which are present only in the flat-spin case.

As the ogive–cylinder is driven at higher and higher spin rate, the Reynolds number is increasing, first reaching the critical value outboard towards the cylinder tip, where the two-bubble separation geometry is established (see Fig. 14). When the spin rate is increased beyond $\Omega = 0.25$, it is possible according to Schewe's results[13] that the subcritical–critical flow separation geometry is established over a limited spanwise extent outboard towards the cylinder tip, whereas the inboard section still has the two-bubble separation geometry. This would explain the decrease of the magnitude of the damping C_n at $0.25 < \Omega < 0.50$. At $\Omega > 0.5$, the one-bubble asymmetric flow separation geometry sketched in Fig. 3 is apparently established, as is illustrated by the flow sketch in Fig. 14. The helical flow stagnation line (Fig. 12) along the span in the case of flat spin (Fig. 14) and the associated three-dimensional flow effects (Fig. 13), together with the spanwise variation of the local Reynolds number discussed earlier, make it very difficult for the same crossflow separation geometry to be established over a large spanwise extent.

Transient Flat-Spin Characteristics

In the flat-spin case, the spin is initiated by static flow separation asymmetry, unevenly distributed along the span. It is obvious that the side force generated outboard towards the tips of the circular cylinder will generate the dominant yawing moment, determining the direction and acceleration of the flat-spin motion. As pointed out by Schewe,[22] it is improbable that transition would occur simultaneously on both sides of the stagnation line. Differences in the flow microstructure on the two sides could arise from any number of sources, of which body microasymmetry and surface roughness are the most obvious. In addition, in the wind tunnel the pressure gradients produced by the support could result in sufficient deceleration of the flow on one side to affect transition. In the case of the free-falling canister this differential effect is probably motion induced.[23] Because of its bistable characteristics the circular cylinder cannot trim at $\alpha = 90$ deg, but will precess about a slightly smaller mean AOA, providing the fluctuating flow separation conditions that could lead to flat-spin initiation. The process leading to the one-bubble configuration can involve many phases of instability,[22] which might be highly sensitive to freestream turbulence.

It is possible that the symmetric, two-bubble critical flow separation may develop momentarily on some spanwise segment, generating the negative, damping, yawing moment contribution measured at $0.25 < \Omega < 0.50$ (Ref. 17) (Fig. 14). The pure damping contribution, generated by the two-bubble separation geometry when driving the model at $\Omega < 0.25$, is probably next to impossible to establish in the free-to-spin case. It could possibly be established on some spanwise segment, in which case something similar to the transient condition at $0.25 < \Omega < 0.50$ in Fig. 14 could occur very briefly over a limited spanwise extent on the free-to-spin circular cylinder.

In the free-to-spin test[24] (Fig. 15), as in the case of the two-dimensional cylinder,[13] increasing or decreasing the Reynolds number establishes the same type of asymmetric supercritical–critical flow separation, resulting in the same magnitude of the maximum flat-spin rate (compare + and × symbols in Fig. 15). And, as in the two-dimensional case[13] (Fig. 7), the peak sectional side force is of the same magnitude for increasing and decreasing Reynolds number, resulting in the same maximum flat-spin rate for increasing and decreasing Reynolds numbers. Based upon Schewe's results[13] (Fig. 7) the supercritical–critical flow separation in the presence of large upstream moving wall effects, sketched in Fig. 14 for $\Omega \geq 0.6$, is very similar to the subcritical–critical separation asymmetry in the presence of downstream moving wall effects, sketched in Fig. 4 for $0.1 < U_W/U_\infty < 0.2$, producing lift forces of the same magnitude. Consequently, one could assume that the maximum local side force for the supercritical–critical separation asymmetry in the flat-spin case ($\Omega > 0.6$ in Fig. 14) will be of the same magnitude as the Magnus lift for subcritical–critical flow separation asymmetry ($\Omega < 0.2$ in Fig. 4). This is the assumption implicit in the flat-spin prediction method derived in Ref. 9. Similarly, it is assumed in Ref. 9 that the maximum moving wall effects on a rotating circular cylinder at critical flow conditions, curves j, k, and l in Fig. 4, obtained for $U_W/U_\infty < 0.2$, are approximately the same as those for a translating cylinder at $\Omega \leq 1$ in Fig. 14, where $U_W/U_\infty = \eta\Omega$. How can this be the case?

In Ref. 25 it is shown that the potential separation delay and associated increase of airfoil maximum lift, generated by the moving wall effects on the boundary-layer buildup near the flow stagnation point, is rapidly saturated with increasing pitch rate. This saturation phenomenon should also apply to the effect of spin rate on the rotating circular cylinder, although the saturation level of U_W/U_∞ might be slightly higher because of the three-dimensional flow effects. However, as already noted, in a first approximation one can use the results for $U_W/U_\infty <$ 0.2 in Fig. 4 to represent the moving wall effects for a translating cylinder. For $U_W/U_\infty > 0.2$ in Fig. 4, the moving wall effects on the boundary-layer development away from the flow stagnation point become important. At $U_W/U_\infty \geq 2$, they are strong enough to prevent the usual flow separation with associated von Kármán vortex shedding from occurring on the rotating cylinder.[26] For this reason, the peak negative Magnus lift measured for subcritical–critical flow separation at $0.1 < U_W/U_\infty < 0.2$ in Fig. 4 was used in Ref. 9 to represent the

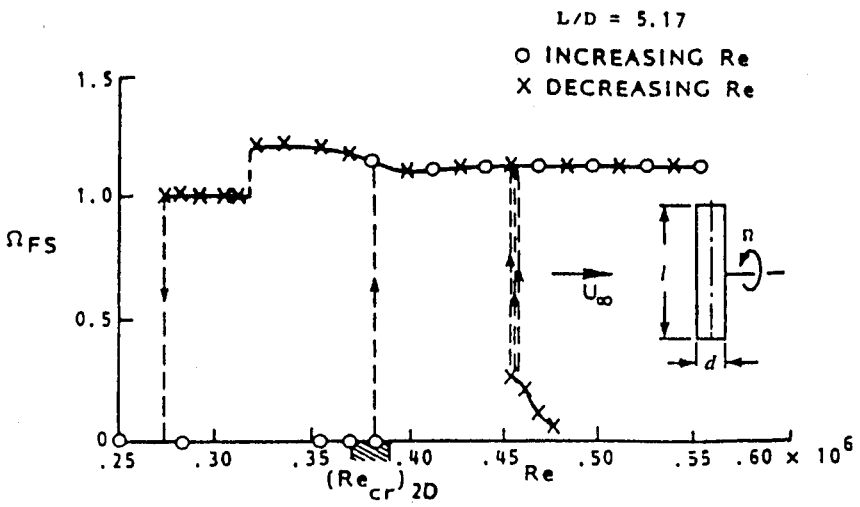

Fig. 15 Flat spin of a circular cylinder for increasing and decreasing Reynolds number.[24]

sectional side force for the translating circular cross section at $0.6 \leq \Omega \leq 1.0$ in Fig. 14, when it experiences the supercritical–critical flow separation indicated by the inset sketch.

The detailed description of the relationship between the moving wall effects on a circular cylinder in flat spin and those generating Magnus lift on a rotating cylinder, together with the envisioned three-dimensional flow effects, provide a sound basis for the extension of the prediction method derived in Ref. 9 to develop a more realistic prediction of the flat spin of a circular cylinder in free fall.

Conclusions

An examination of the fluid mechanics of the flat spin of a circular cylinder led to the following conclusions:

1) Flat spin is maintained by the supercritical–critical crossflow separation generated by the moving wall effect at critical flow conditions, facilitated by the spanwise venting of the flow separation through three-dimensional flow effects. The moving wall effect controls the crossflow separation through its effect on boundary-layer transition.

2) In regard to the initiation of flat spin, it is found that minute surface roughness plays a dominating role, generating a large autorotative moment that almost instantaneously accelerates the circular cylinder up to the final, large flat-spin rate.

3) The three-dimensional flow topology and flowfield interactions described provide the basis for the development of a more refined prediction method for flat spin of a circular cylinder than previously possible.

References

[1]Ericsson, L. E., and Beyers, M. E., "Flat Spin of Axisymmetric Bodies," *Journal of Aircraft*, Vol. 32, No. 6, 1995, pp. 1205–1212.

[2]Ericsson, L. E., "Moving Wall Effects in Unsteady Flow," *Journal of Aircraft*, Vol. 25, No. 11, 1988, pp. 977–990.

[3]Yoshinaga, T., Tate, A., and Inoue, K., "Coning Motion of Slender Bodies at High Angles of Attack," AIAA Paper 81-1899, Aug. 1981.

[4]Ericsson, L. E., and Reding, J. P., "Asymmetric Flow Separation and Vortex Shedding on Bodies of Revolution," *Tactical Missile Aerodynamics: General Topics*, edited by M. J. Hemsch, Vol. 141, Progress in Astronautics and Aeronautics, AIAA, Washington, DC, 1992, pp. 391–452, Chap. 10.

[5]Ericsson, L. E., "Prediction of Slender Body Coning Characteristics," *Journal of Spacecraft and Rockets*, Vol. 28, No. 1, 1991, pp. 43–49.

[6]Kubota, H., Irai, I., and Matsuaka, M., "Wind Tunnel Investigations for the Flat Spin of Slender Bodies at High Angles of Attack," *Journal of Spacecraft and Rockets*, Vol. 20, No. 2, 1983, pp. 108–114; also AIAA Paper 82-0054, Jan. 1982.

[7]Bearman, P. W., "On Vortex Shedding from a Circular Cylinder in the Critical Reynolds Number Regime," *Journal of Fluid Mechanics*, Vol. 37, Pt. 3, 1969, pp. 577–585.

[8]Yoshinaga, T., and Tate, A., "Flat Spin of Slender Bodies near the Critical Reynolds Number Region," private communication, Dec. 1985.

[9]Ericsson, L. E., "Flat Spin of Axisymmetric Bodies in the Critical Flow Region," *Journal of Spacecraft and Rockets*, Vol. 24, No. 6, 1987, pp. 532–538.

[10]Achenbach, E., "Influence of Surface Roughness on the Cross-Flow Around a Circular Cylinder," *Journal of Fluid Mechanics*, Vol. 46, Pt. 2, 1971, pp. 321–335.

[11]Swanson, W. M., "Magnus Effect; A Summary of Investigations to Date," *Journal of Basic Engineering*, Vol. 83, Sept. 1961, pp. 461–470.

[12]Kamiya, N., Susuki, S., and Nishi, T., "On the Aerodynamic Force Acting on a Circular Cylinder in the Critical Range of the Reynolds Number," AIAA Paper 79-1475, July 1979.

[13]Schewe, G., "Sensitivity of Transition Phenomena to Small Perturbations in Flow Around a Circular Cylinder," *Journal of Fluid Mechanics*, Vol. 172, 1986, pp. 33–46.

[14]Bearman, P. W., and Harvey, J. K., "Control of Circular Cylinder Flow by the Use of Dimples," *AIAA Journal*, Vol. 31, No. 10, 1993, pp. 1753–1756.

[15]Schlinker, R. H., Fink, M. R., and Amiet, R. K., "Vortex Noise from Non-Rotating Cylinder and Airfoils," AIAA Paper 76-81, Jan. 1976.

[16]Schechenyi, E., "Supercritical Reynolds Number Simulation for Two-Dimensional Flow over Circular Cylinders," *Journal of Fluid Mechanics*, Vol. 70, Pt. 3, 1975, pp. 529–542.

[17]Ericsson, L. E., and Beyers, M. E., "Viscous-Flow/Vehicle-Motion Coupling," *Fluid Dynamics of Rotor Flows, Rotary-Balance Testing for Aircraft Dynamics*, AGARD-AR-265, Dec. 1990, pp. 164–167, 183–187, Chap. 8.

[18]Dallmann, U., and Schewe, G., "On Topological Changes of Separating Flow Structures at Transitional Reynolds Numbers," AIAA Paper 87-1266, June 1987.

[19]McLaughlin, T. E., Stephen, E. J., and Robinson, M. C., "Pressure Measurements on a Rotating Cylinder," AIAA Paper 91-3265, Aug. 1991.

[20]Ericsson, L. E., and Reding, J. P., "Criterion for Vortex Periodicity in Cylinder Wakes," *AIAA Journal*, Vol. 17, No. 9, 1979, pp. 1012, 1013.

[21]Schlichting, H., "Boundary Layer Theory," McGraw–Hill, New York, 1955, p. 16.

[22]Schewe, G., "On the Force Fluctuations on a Circular Cylinder in Crossflow from Subcritical up to Transcritical Reynolds Numbers," *Journal of Fluid Mechanics*, Vol. 133, 1983, pp. 265–285.

[23]Beyers, M. E., "Interpretation of Experimental High-Alpha Aerodynamics-Implications for Flight Prediction," AIAA Paper 93-0166, Jan. 1993.

[24]Yoshinaga, T., private communication, March 1987.

[25]Ericsson, L. E., "Moving Wall Effect in Relation to Other Unsteady Flow Mechanisms in Dynamic Airfoil Stall," *Journal of Aircraft*, Vol. 31, No. 6, 1994, pp. 1303–1309.

[26]Diaz, F., Gavalda, J., Kawall, J. G., Keller, J. F., and Giralt, F., "Vortex Shedding from a Spinning Cylinder," *Physics of Fluids*, Vol. 26, Dec. 1983, pp. 3454–3460.